Journal of Magnetic Resonance 298 (2019) 85–90

Contents lists available at ScienceDirect

Journal of Magnetic Resonance

journal homepage: www.elsevier.com/locate/jmr

Detection of liquids by magnetic resonance force microscopy in the gradient-on-cantilever geometry

Sebastian Schnoz, Alexander Däpp, Andreas Hunkeler, Beat H. Meier *

Physical Chemistry, ETH Zürich, Vladimir-Prelog-Weg 2, CH-8093 Zurich, Switzerland

ARTICLE INFO

Article history:
Received 5 September 2018
Revised 23 November 2018
Accepted 25 November 2018
Available online 26 November 2018

Keywords:
Magnetic-resonance-force-detection
MRFM
Liquids

ABSTRACT

We demonstrate the detection of picoliter amounts of water and triethylenetetramine by a magnetic-resonance-force-microscopy (MRFM) setup operated in the gradient-on-cantilever geometry at room temperature. A magnetic field gradient is produced by a ferromagnetic SmCo particle glued to the tip of a micromechanical resonator (cantilever). The liquids are enclosed in a micro-capillary to protect them from the high vacuum environment needed for sensitive detection. We describe simple spectroscopic experiments as proton T_1 – relaxation, Rabi nutation curves and Hahn-echo measurements.

1. Introduction

Magnetic resonance force microscopy (MRFM) is a method to detect magnetic resonance signals by means of force detection via a micromechanical resonator [1,2]. Compared to inductively detected magnetic resonance, force detection is more sensitive when decreasing the sample size to the low micrometer and down to the nanometer range [3]. So far, MRFM was mainly performed on solid samples. As an exception, Madsen et al. measured nuclear magnetic resonance (NMR) on a 9 µl sample of water by force detection in a homogeneous magnetic field [4].

An MRFM experiment is performed in a strong external magnetic field which aligns the spin magnetization of the sample (attached typically to the tip of the cantilever) parallel to the external magnetic field. The basic principle of force detection of magnetic resonance by MRFM is the interaction of the spin magnetization with the gradient field produced by a nearby ferromagnetic particle. This interaction is mediated by a force proportional to the magnetic moment of the spins and the field gradient. The sign of this force depends on the alignment of the spin magnetization parallel or antiparallel to the external magnetic field and causes the cantilever to bend in either direction. Periodically inverting the spin magnetization at the mechanical cantilever eigenfrequency leads to a driven damped harmonic oscillation of the cantilever whose amplitude can be detected by laser beam deflection [5,6]. To obtain the necessary high Q factors for sensitive detection, the cantilever and sample are placed in vacuum.

While for MRFM of solid samples the sample is often placed on the cantilever and the gradient source is fixed with respect to the laboratory frame (sample-on-cantilever design), this setup is difficult to realize for liquid samples. Because of the small dimensions of the cantilever, a micron-sized vacuum protection chamber is necessary that protects the liquid from the high vacuum. Suitable vacuum sealed micro-containers are hard to produce and might complicate the sample preparation. Therefore, the change from the sample-on-cantilever to the gradient-on-cantilever geometry simplifies the sample handling and allows the sample size not to be restricted by the size of the cantilever. In the gradient-on-cantilever geometry the ferromagnetic particle producing the magnetic gradient field is glued to the tip of the cantilever whereas the sample is placed close to it. This design was first realized by Wago et al. with the cantilever motion parallel to the external magnetic field [7]. Unfortunately, the demonstrated design caused a severe degradation of the cantilever's quality factor inside the magnet due to the restoring force acting on it. A solution to this problem was introduced by Marohn et al. by applying the field in a direction perpendicular to the direction of the cantilever motion (SPAM) [8–10]. The interchange of the position of the magnetic particle and the sample compared to the sample-on-cantilever geometry leaves the detection principle unchanged.

We demonstrate the detection of two different liquids (water and triethylenetetramine (TETA)) in the picoliter range (~10–60 picoliter) using the SPAM geometry. This is a significant reduction in detectable sample amounts by about one to three orders of magnitude compared to inductively detected techniques [11–13],

* Corresponding author.
E-mail address: beme@ethz.ch (B.H. Meier).

https://doi.org/10.1016/j.jmr.2018.11.009
1090-7807/

where micro-coils and striplines are combined with micro-fluidics. Methods based on optically detected NMR by using a nitrogen vacancy in diamond as a sensor showed a detection of only 20 zeptoliter in sample volume [14]. While this method is much more sensitive, only sample volumes within less than 100 nm from the sensor could be detected whereas our method addresses samples at a distance of several micrometers.

In our test experiments the liquid samples are enclosed in micro-capillaries to protect the liquids from the high vacuum environment. T_1-inversion recovery, Hahn-echo and nutation experiments are described in this work as proof of principle for measuring the proton spin magnetization of the samples.

In the future, this may allow for the detection of small amounts of liquids and liquid containing samples (i.e., a single biological cell and compartments thereof, liquids inside a micropore) in the picoliter and the femtoliter range.

2. Experimental setup

In the presented work we operate our home-built MRFM setup (at room temperature) in the gradient-on-cantilever geometry (Fig. 1(a)) where we seal our (liquid) samples in quartz capillaries (G-1 glass capillaries, Narishige Japan) that are pulled to an inner diameter of about 20 μm and a wall thickness of about 5 μm at the tip (PC-10 dual-stage glass micropipette puller, Narishige Japan), as shown in Fig. 1(b) and (c). A small amount of liquid is injected into the capillary and spun down to the tip by a centrifuge. For our experiments we used water and triethylenetetramine (Sigma-Aldrich) as samples. The tip end of the capillary is closed by melting the glass whereas the wide end is sealed by fast hardening glue (Cementit Universal, merz + benteli ag). A nearby cantilever (Veeco Instruments, MLCT-NOHW) with a magnetic particle (SmCo, ~40 μm × 40 μm × 80 μm) glued to it (Fig. 1(d) and (e)) probes the magnetic resonance of the sample inside the micro-capillary by inverting the sample's spins periodically at the resonance frequency of the cantilever ($f_{can} \approx 703$ Hz, $k_{can} \approx 2.5$ mN/m, $Q \approx 5000$) and therefore driving the cantilever on resonance. The magnetic particle is placed at a distance of about 30 μm from the sample. Originally, the magnetic particle was unmagnetized. After gluing the particle to the tip of the cantilever the cantilever was placed into the superconducting magnet (external field B_0 of 5.87 T) while the glue was hardening. The magnetization of the SmCo particle is then aligned with the external magnetic field to minimize forces on the cantilever. The cantilever's oscillation amplitude is measured by laser beam deflection [6] and is proportional to the detected spin density [15]. The laser is focused on the tip of the cantilever. The laser beam is reflected onto a position sensitive four quadrant detector (Hamamatsu, Si PIN photodiode S7479). Radio frequency (rf) pulses for manipulation of the spins are achieved by using a micro-coil made of a 50 μm thick copper wire and wound by hand. The micro-coil's diameter is about 200 μm. The experiment was performed in a vacuum environment of about 10^{-4} mbar generated by a turbomolecular pump (Pfeiffer).

3. Results and discussion

3.1. One-dimensional experiments

The magnetic field at the sample's position, B_{Sum}, is the sum of the external magnetic field B_0 and the magnetic field produced by the ferromagnetic particle leading to a Larmor frequency of $\omega_0 = -\gamma B_{Sum}$ (γ is the gyromagnetic ratio of the spin species). Due to the gradient of the magnetic field, the Larmor frequency within the sample changes with position. A region of spins (the resonance slice) can be chosen for detection by defining the carrier frequency and the frequency width of the adiabatic radio frequency inversion pulse during detection (Fig. 2) [16]. A 1D-scan (leading to the sequential detection of a 1D "image") of the sample is measured by acquiring the signal from each resonance slice sequentially. Multiplexed acquisition schemes using Hadamard encoding for MRFM are described elsewhere [17] but were not employed here. The basic 1D-scan pulse sequence is given in Fig. 2. A prepulse and a polarization cycle are applied prior to detection to reduce and average out rf-cantilever interactions. We assume that this led to thermo-mechanical fluctuations in cantilever position as the main source of noise. The thermal tip motion in our experiments is on the order of $z_{rms} \sim 1.3$ nm. The detection sequence consists of a train of adiabatic hyperbolic secant inversion sweeps [18]. The spins are inverted twice per cantilever oscillation period therefore driving the cantilever at its mechanical resonance. The signal of the 1D-scans was recorded with a train of hyperbolic secant inversion sweeps (sweep duration ~700 μs, frequency width 125 kHz (water) and 250 kHz (TETA), truncation parameter of 20)

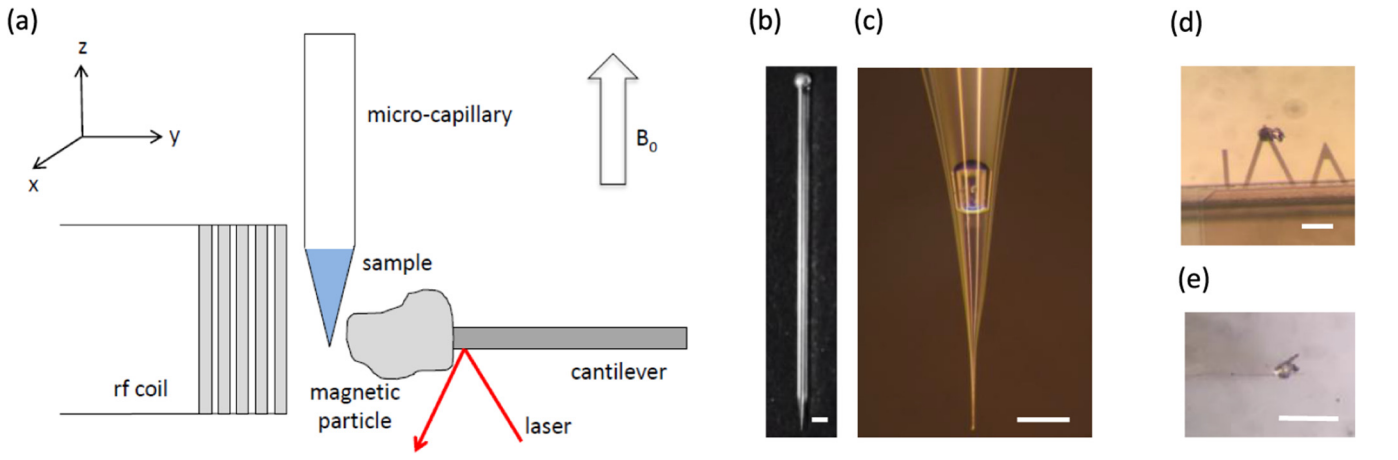

Fig. 1. (a) Schematics of the measurement setup. An external magnetic field B_0 produced by a 5.87 T superconducting magnet aligns the ^{1}H spins of the sample parallel to the z-axis. The liquids are enclosed inside a micro-capillary pulled to form a tip with a narrow wall. A magnetic particle (made of SmCo) is glued to the tip of a cantilever to probe the spin magnetization of the liquids. Radio-frequency pulses are generated by a micro-coil. The cantilever oscillates along the x-axis. (b) Micro-capillary pulled to form a narrow tip with low wall thickness. The tip end is closed by melting the glass, the other end is closed by a drop of fast hardening glue. The scale bar is 1 mm. (c) Tip of a micro-capillary which is filled with water. An air bubble can be seen. The wall thickness of the capillary at the tip is about 5 μm. The scale bar is 500 μm. (d), (e) Cantilever with the SmCo particle glued to the tip viewed from two different sides. Both scale bars are 100 μm.

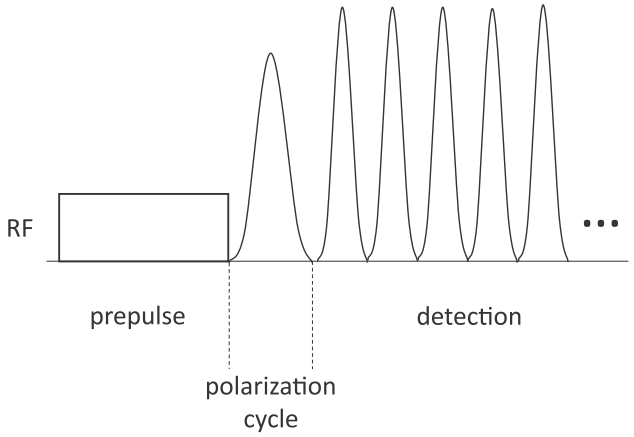

Fig. 2. Basic pulse sequence for a 1D-scan. A prepulse heats up the cantilever for reduced rf-cantilever interaction during the detection period. A polarization cycle averages out rf- cantilever interactions by inverting the spin magnetization prior to every second acquisition. Subtraction of the signals reveals the spin signal but cancels the rf-cantilever interaction. The detection sequence consists of a train of adiabatic inversion sweeps (hyperbolic secant inversion sweeps in our experiments [18]). The spins are inverted twice per cantilever cycle.

with a mean amplitude of about 70 kHz over the detected region and a detection time of 1 s. 80 scans were recorded for water and 20 scans for TETA for signal averaging.

The signal-to-noise ratio (SNR) of an MRFM measurement in the amplitude-modulation detection scheme is given by [15,19]:

$$SNR = M_0 \cdot \partial_i B_z \cdot \sqrt{\frac{Q\pi f_{can}}{2k_{can}k_B T}} \cdot \sqrt{T^*_{1\rho}} \qquad (1)$$

where M_0 is the Boltzmann equilibrium magnetization and depends linearly on the spin density inside the detected resonance slice. The gradient field $\partial_i B_z$ is produced by the ferromagnetic particle where the index $i = \{x, y, z\}$ corresponds to the direction along which the cantilever is oscillating. In our experiment i equals x. Furthermore, the sensitivity depends on the cantilever frequency f_{can}, the spring constant k_{can} and the quality factor Q of the cantilever. The temperature T goes into the equation since the temperature influences the thermal noise of the cantilever. Additionally, the magnetization M_0 is inversely proportional to the temperature T; k_B is the Boltzmann constant. The $T_{1\rho}$ is the spin-lock decay time during the cyclic adiabatic inversion sweeps of the detection period. It enters the equation as square root because the longer the detection period the more white noise is recorded.

In Fig. 3, a 1D-scan of capillaries filled with water and TETA is shown. The signal is plotted as a function of the resonance slice center Larmor frequency. If the shape of the magnetic particle and therefore the magnetic gradient field were well defined, it would be possible to calculate a spatial position coordinate from the Larmor frequency coordinate. For our experiment a gradient source of irregular shape was used, however, and the information is only approximate. An approximate value for the magnetic gradient strength in our experiment is 147 T/m. There is only one signal point in Fig. 3(a) for water, whereas in Fig. 3(b) three signal points are detected for TETA (for the same amount of sample). The reason is the two orders of magnitude higher self-diffusion coefficient of water which causes the spins to flow out of (and possibly reenter, but with different phase because they missed inversion pulses) the detected slice during the detection period much faster than in the case of TETA, if the resonance slice covers the sample's volume only partially. This process causes a decay of the spin magnetization during detection (additional to $T_{1\rho^*}$), phenomenologically described by a relaxation time T_{Diff} that can be determined by simulations as described below.

We first investigate the signal still detectable from a slice with a dimension of micrometers being part of a larger sample. We assume that we need T_{Diff} to be longer than 10 ms to detect the signal from the slice [19]. Restricting ourselves to one dimension for this simple estimation, this leads to a minimum detectable slice thickness of around 18 µm for water and 2 µm for TETA (see Fig. S2(a) and S5(a) of the SI). For the details of the calculation see supporting information. For restricted samples, the situation is different. If the entire sample is contained in the detection slice, no diffusion contribution exists, but already for the case of a water sample of dimension 20 µm, selecting a resonance slice with a width of 18 µm in the center of the sample volume will result in a T_{Diff} of only 16.5 ± 0.1 ms (Fig. S3(a)) very close to the value of a large sample of 1000 µm dimension (16.6 ± 0.2 ms, Fig. S2(a)). Note that for a 20 µm slice, T_{Diff} goes towards infinity.

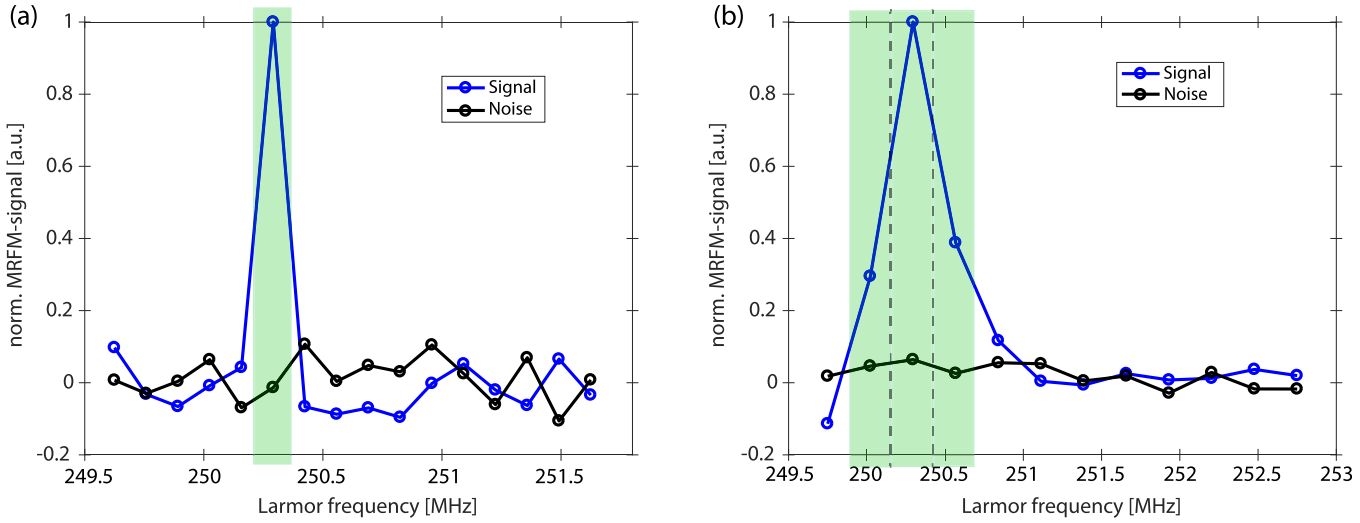

Fig. 3. Force-detected magnetic resonance signals of water (a) and TETA (b) are shown. There is only one signal point for water since the self-diffusion of spins into and out of small resonance slices decreases the signal intensity to a non-detectable value (further explanations can be found in the text). The resonance slices are indicated by green areas. Resonance slices have a width of 125 kHz for water and 250 kHz for TETA. The black traces contain noise with an estimated amplitude (see text) of $z_{rms} \sim \sqrt{N} * 1.3$ nm. The maximum signal in (b) is about 1.6 times smaller than the signal in (a). N = 80 scans and 20 scans were recorded for water and TETA, respectively. Therefore the signal per scan is 2.5 times larger for the TETA signal. (For interpretation of the references to color in this figure legend, the reader is referred to the web version of this article.)

The calculations are based on numerically solving the diffusion equation (Fick's second law) in MATLAB (Mathworks, Cambridge, UK). For the simulation, the inversion pulses are assumed to be in the delta pulse limit and are applied each half cantilever period. The simulated magnetization decay curve is fitted by an exponential function $\sim e^{-t/T_{Diff}}$ to get a value for T_{Diff}. The self-diffusion coefficient of water is about $D = 2.3 \times 10^{-9}$ m^2/s at 25 °C [20].

For water, the resonance slice must cover at least 18 μm (for large sample volumes) or the entire (for small sample volumes) liquid sample to be detectable with reasonable sensitivity. For TETA, the much slower self-diffusion ($D \approx 4 \times 10^{-11}$ m^2/s) makes it possible to measure the signal from a much thinner resonance slice. For example, taking a 2 μm thick resonance slice within a TETA sample dimension of 20 μm (restricting ourselves to one dimension) leads to a signal decay T_{Diff} of about 12.6 ± 0.2 ms (Fig. S7 (a)). Such a signal is still detectable with the amplitude-modulation detection scheme. Therefore for TETA, three signal points from resonance slices covering the sample's volume only partially were experimentally detected. Note that for self-diffusion into and out of the resonance slice in all three dimensions, the signal decay is enhanced compared to the 1D-restricted case and the width of the slice might even have to be bigger for sensitive detection. In our experiments, the resonance slices are of such a shape that one dimension is much smaller than the other two. Therefore, the treatment of the diffusion problem in one dimension is justified.

We estimate the detection volume to be around 60 picoliter for water and between 10 and 60 picoliter for TETA. For water, the estimation is based on a resonance slice covering a cylindrical volume with diameter of 20 μm (inner diameter of the capillary) and a length of 200 μm (diameter of the rf coil) where spins are affected by the inversion sweeps during detection. For TETA, the three signal points arise from resonance slices covering only a small spatial width within the bulk liquid. It's worth mentioning that due to the nonlinearity of the magnetic gradient field the resonance slices get thinner closer to the magnetic particle.

3.2. T_1 – inversion recovery experiments

During a T_1-inversion recovery experiment, the spin magnetization is inverted by an adiabatic inversion sweep (hyperbolic secant sweep, sweep duration 0.5 ms, average amplitude ~45 kHz, truncation parameter 20) and allowed to relax during a T_1 delay time prior to detection (Fig. 4). For TETA (Fig. 4(a)), a T_1 value of about 170 ± 40 ms was determined. A reference value of 340 ± 10 ms was measured on a 300 MHz spectrometer (Bruker Avance II). For water (Fig. 4(b)) a T_1 value of about 1.9 ± 0.2 s was determined. A reference value for the proton T_1 relaxation time of about 2.93 ± 0.01 s was measured at room temperature and a field of 300 MHz (Bruker Avance II). Deviations might result from paramagnetic impurities (including oxygen) and differences in temperature. It is important to mention that if the detected resonance-slice for the T_1-inversion recovery experiment covers the sample volume only partially, the T_1 time can be distorted from the real value by diffusion of molecules into/out of the slice during the T_1-delay time. The T_1-inversion recovery experiments for TETA were therefore set up in such a way that the detected region was much smaller (250 kHz) than the inverted region (500 kHz). In this way the spins diffusing into or out of the resonance slice during the time of the T_1 relaxation have the same magnetization.

3.3. Nutation and Hahn-echo experiment

In Fig. 5 a proton nutation experiment (Fig. 5(a)) and a proton Hahn-echo experiment (Fig. 5(b)) of water are shown [21]. The nutation curve was measured by applying a radio frequency-pulse with an average amplitude B_1 over the detected resonance slice of about 100 kHz along the x-axis. The duration of the pulse was incremented in steps of 0.4 μs. The fast decay of the nutation curve is ascribed to the field inhomogeneity of the nutation pulse over the detected resonance slice. This is illustrated by the red trace in Fig. 5(a) corresponding to the nutation curve obtained for a Gaussian distribution of field strength (center 105 kHz, FWHM 67 kHz). Furthermore, self-diffusion of the spins during the nutation pulse might further shorten the decay time.

As it can be seen from Fig. 5(b), the echo signal decays after about 100 μs. Normally in a Hahn-echo decay experiment of water the signal life time is up to several seconds [22]. However, in the presence of a field gradient, the diffusion in the liquid interferes with the echo formation and leads to the faster decay [21,23–25]. Since we know the self-diffusion coefficient of water, we can use the formula describing the decay of the echo signal given by Stejskal and Tanner and calculate the magnetic gradient strength from our data. The decay of the signal intensity I during a Hahn-echo due to self-diffusion in an inhomogeneous static magnetic field is given by

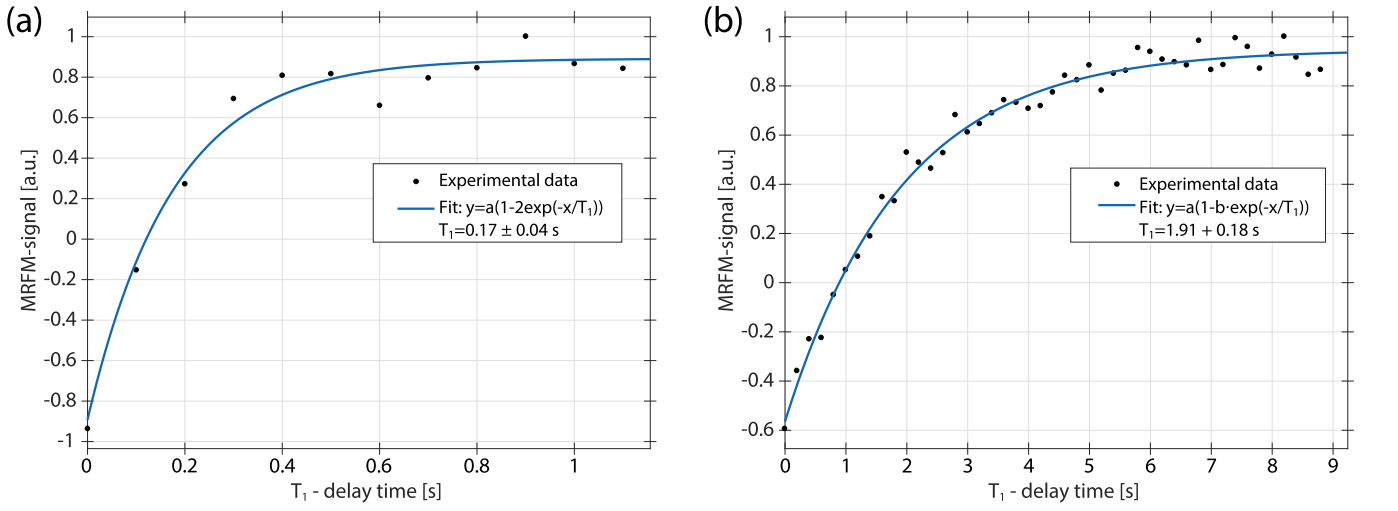

Fig. 4. T_1 – inversion recovery experiments are shown of TETA (a) and water (b). The black dots are the measured data points of the inversion recovery experiment. The blue line is an exponential fit according to the function given in the legend of the Figures. (For interpretation of the references to color in this figure legend, the reader is referred to the web version of this article.)

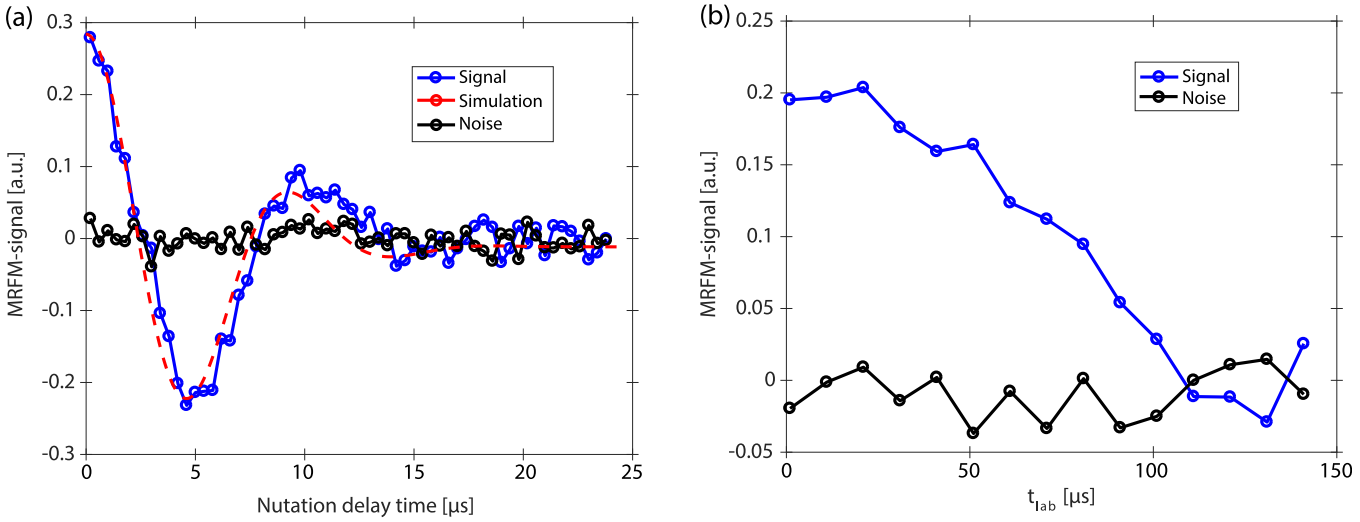

Fig. 5. Signals from a nutation experiment (a) and a Hahn-echo experiment (b) for water protons. The fast decay of the nutation curve is due to the field inhomogeneity of the nutation pulse B_1 along the x-axis and is illustrated by the red line which simulates a Gaussian distribution of rf-field strength. The Hahn-echo decay is governed by the self-diffusion in the inhomogeneous static magnetic field. (For interpretation of the references to color in this figure legend, the reader is referred to the web version of this article.)

$$I(\tau) = I_0 \exp\left(\frac{-2}{3}\gamma^2 G_0^2 \tau^3 D - 2\frac{\tau}{T_2}\right) \quad (2)$$

where γ is the gyromagnetic ratio, G_0 is the gradient strength, τ is the Hahn-echo decay time, D is the self-diffusion coefficient and T_2 is the transverse relaxation time. The second term in the exponential can be neglected since $\tau \ll T_2$ in our experiment ($\tau \approx 100$ μs, $T_2 \approx 1$ s). Rearranging Eq. (2) leads to

$$\ln\left(\frac{I}{I_0}\right) \approx \frac{-2}{3}\gamma^2 G_0^2 \tau^3 D \quad (3)$$

Plotting the data given in Fig. 5(b) according to Eq. (3) allows to calculate the gradient strength G_0 from the slope of the linear fit which gives a value of 127 ± 11 T/m (Fig. 6). This is compatible with estimations of the thickness of the slice (20 μm) and its frequency width (125 kHz) (assuming that the strongest gradient is along the x-axis) which yields 147 T/m.

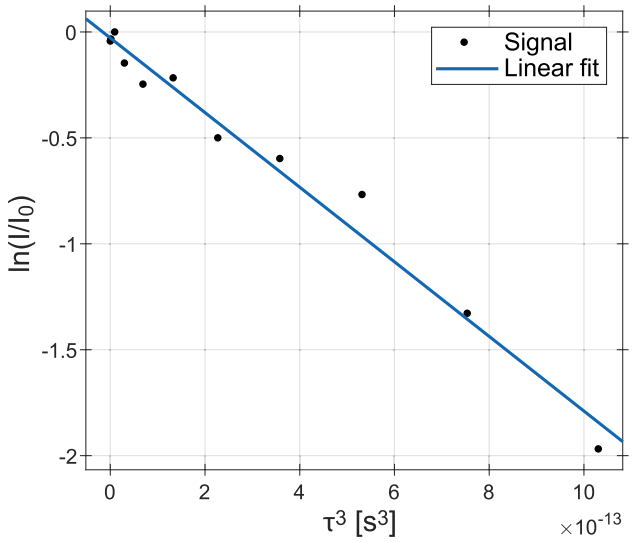

Fig. 6. Normalized signal intensity of the Hahn-echo decay signal from Fig. 5(b) plotted as a function of the third power of the dephasing time τ. Since the self-diffusion coefficient of water is known [20] the magnetic gradient strength $G_0 = 127 \pm 11$ T/m can be calculated from the slope of the linear fit (according to Eq. (3)).

4. Conclusions

We explored the use of the micro-capillaries as a vacuum protection system for detection of liquid samples by MRFM using a gradient-on-cantilever setup. A Hahn-echo experiment shows the effect of the self-diffusion of spins on the signal decay and the limits of resolution when the inhomogeneous magnetic field is present. Strong dephasing effects appear when the image slice is smaller than the diffusion length during the detection period of typically 0.07–0.5 s (the diffusion-length of water is about 18 μm in 0.07 s and about 2 μm in 0.07 s for TETA for 1D-restricted diffusion). The spatial resolution in our setup (restricted to one dimension) of bulk water is limited to about 18 μm whereas for bulk TETA with a two orders of magnitude lower self-diffusion coefficient, a spatial resolution of about 2 μm is possible. For comparison, the spatial resolution of micro-MRI is limited to a few micrometers for bulk water [26]. However, one is mostly not interested in imaging slices out of bulk liquids. Interesting samples such as single biological cells show some kind of structure or compartmentalization which hinders the self-diffusion of liquids compared to the bulk liquid [27,28]. The cytoplasm of cells contains a mixture of compounds which show self-diffusion coefficients between the one of bulk water and down to about 10^{-12} m^2/s [29]. Furthermore, cells show low-mobility structures such as the cell wall, the cytoskeleton or the organelles. Therefore, a spatial resolution of about 1 μm or even lower may be feasible in some systems.

Acknowledgments

The authors would like to thank the Schweizerische Nationalfonds (SNF, grants 200020_178792 and 200020_159707) for financial support. We thank Prof. Christian Degen for providing the glass capillaries and the capillary puller. Special thanks go to Dr. Fei Xue for fruitful discussions about protecting liquids from vacuum environments.

Appendix A. Supplementary material

Supplementary data associated with this article can be found, in the online version, at https://doi.org/10.1016/j.jmr.2018.11.009.

References

[1] J.A. Sidles, Noninductive detection of single-proton magnetic-resonance, Appl. Phys. Lett. 58 (1991) 2854–2856.
[2] D. Rugar, C.S. Yannoni, J.A. Sidles, Mechanical detection of magnetic resonance, Nature 360 (1992) 563.
[3] J.A. Sidles, D. Rugar, Signal-to-noise ratios in inductive and mechanical detection of magnetic resonance, Phys. Rev. Lett. 70 (22) (1993) 3506–3509.
[4] L.A. Madsen, G.M. Leskowitz, D.P. Weitekamp, Observation of force-detected nuclear magnetic resonance in a homogeneous field, Proc. Natl. Acad. Sci. USA 101 (35) (2004) 12804–12808.
[5] A. Schaff, W.S. Veeman, Mechanically detected nuclear magnetic resonance at room temperature and normal pressure, J. Magn. Reson. 126 (1997) 200–206.
[6] G. Meyer, N.M. Amer, Novel optical approach to atomic force microscopy, Appl. Phys. Lett. 53 (24) (1988) 2400.
[7] K. Wago, D. Botkin, C.S. Yannoni, D. Rugar, Paramagnetic and ferromagnetic resonance imaging with a tip-on-cantilever magnetic resonance force microscope, Appl. Phys. Lett. 72 (1998) 2757.
[8] J.A. Marohn, R. Fainchtein, D.D. Smith, An optimal magnetic tip configuration for magnetic-resonance force microscopy of microscale buried features, Appl. Phys. Lett. 73 (1998) 3778.
[9] D.D. Smith, J.A. Marohn, L.E. Harrell, Detailed description of a compact cryogenic magnetic resonance force microscope, Rev. Sci. Instrum. 72 (2001) 2080.
[10] S.R. Garner, S. Kuehn, J.M. Dawlaty, N.E. Jenkins, J.A. Marohn, Force-gradient detected nuclear magnetic resonance, Appl. Phys. Lett. 84 (2004) 5091.
[11] A.P.M. Kentgens, J. Bart, P.J.M. van Bentum, A. Brinkmann, E.R.H. van Eck, J.G.E. Gardeniers, J.W.G. Janssen, P. Knijn, S. Vasa, M.H.W. Verkuijlen, High-resolution liquid- and solid-state nuclear magnetic resonance of nanoliter sample volumes using microcoil detectors, J. Chem. Phys. 128 (2008) 052202.
[12] J. Bart, J.W. Janssen, P.J. van Bentum, A.P.M. Kentgens, J.G.E. Gardeniers, Optimization of stripline-based microfluidic chips for high-resolution NMR, J. Magn. Reson. 201 (2) (2009) 175–185.
[13] E. Montinaro, M. Grisi, M.C. Letizia, L. Pethö, M.A.M. Gijs, R. Guidetti, J. Michler, J. Brugger, G. Boero, 3D printed microchannels for sub-nL NMR spectroscopy, PLoS One 13 (5) (2018), https://doi.org/10.1371/journal-pone.0192780 e0192780.
[14] N. Aslam, M. Pfender, P. Neumann, R. Reuter, A. Zappe, F.F. de Oliveira, A. Denisenko, H. Sumiya, S. Onoda, J. Isoya, J. Wrachtrup, Nanoscale nuclear magnetic resonance with chemical resolution, Science 357 (6346) (2017) 67–71.
[15] N. Nestle, A. Schaff, W.S. Veeman, Mechanically detected NMR, an evaluation of the applicability for chemical investigations, Prog. Nucl. Magn. Reson. Spectrosc. 38 (2001) 1–35.
[16] C.L. Degen, Q. Lin, A. Hunkeler, U. Meier, M. Tomaselli, B.H. Meier, Microscale localized spectroscopy with a magnetic resonance force microscope, Phys. Rev. Lett. 94 (2005) 207601.
[17] K.W. Eberhardt, C.L. Degen, B.H. Meier, Fast magnetic resonance force microscopy with Hadamard Encoding, Phys. Rev. B 76 (2007) 180405.
[18] E. Kupce, R. Freeman, Optimized adiabatic pulses for wideband spin inversion, J. Magn. Reson., Ser. A 118 (1996) 299–303.
[19] C.L. Degen, Magnetic resonance force microscopy: NMR spectroscopy on the micro- and nanoscale, ETH Zürich, Diss. No. 17562, 2008.
[20] M. Holz, S.R. Heil, A. Sacco, Temperature-dependent self-diffusion coefficients of water and six selected molecular liquids for calibration in accurate 1H NMR PFG measurements, PCCP 2 (2000) 4740–4742.
[21] E.L. Hahn, Spin echoes, Phys. Rev. 80 (1950) 580.
[22] D.C. Chang, F. Hazelwood, B.L. Nichols, H.E. Rorschach, Spin echo studies on cellular water, Nature 235 (1972) 170.
[23] H.Y. Carr, E.M. Purcell, Effect of diffusion on free precession in nuclear magnetic resonance experiments, Phys. Rev. 94 (1954) 630.
[24] E.O. Stejskal, J.E. Tanner, Spin diffusion measurements: spin echoes in the presence of a time-dependent field gradient, J. Chem. Phys. 42 (1965) 288.
[25] D.G. Rata, F. Casanova, J. Perlo, D.E. Demco, B. Blümich, Self-diffusion measurements by a mobile single-sided NMR sensor with improved magnetic field gradient, J. Magn. Reson. 180 (2) (2006) 229–235.
[26] L. Ciobanu, D.A. Seeber, C.H. Pennington, 3D MR microscopy with resolution 3.7 μm by 3.3 μm by 3.3 μm, J. Magn. Reson. 158 (1–2) (2002) 178–182.
[27] M. Hoppert, F. Mayer, Principles of macromolecular organization and cell function in bacteria and archaea, Cell Biochem. Biophys. 31 (1999) 247.
[28] I. Aslund, D. Topgaard, Determination of the self-diffusion coefficient of intercellular water using PGSE NMR with variable gradient pulse length, J. Magn. Reson. 201 (2009) 250–254.
[29] A. Nenninger, G. Mastroianni, C.W. Mullineaux, Size dependence of protein diffusion in the cytoplasm of Escherichia coli, J. Bacteriol. 192 (18) (2010) 4535–4540.